ELSEVIER

Journal of Contaminant Hydrology 57 (2002) 161–187

JOURNAL OF Contaminant Hydrology

www.elsevier.com/locate/jconhyd

Virus transport in physically and geochemically heterogeneous subsurface porous media

Subir Bhattacharjee [1], Joseph N. Ryan [2], Menachem Elimelech*

Department of Chemical Engineering, Environmental Engineering Program, PO Box 208286, Yale University, New Haven, CT 06520-8286, USA

Received 23 March 2001; received in revised form 29 January 2002; accepted 15 February 2002

Abstract

A two-dimensional model for virus transport in physically and geochemically heterogeneous subsurface porous media is presented. The model involves solution of the advection–dispersion equation, which additionally considers virus inactivation in the solution, as well as virus removal at the solid matrix surface due to attachment (deposition), release, and inactivation. Two surface inactivation models for the fate of attached inactive viruses and their subsequent role on virus attachment and release were considered. Geochemical heterogeneity, portrayed as patches of positively charged metal oxyhydroxide coatings on collector grain surfaces, and physical heterogeneity, portrayed as spatial variability of hydraulic conductivity, were incorporated in the model. Both layered and randomly (log-normally) distributed physical and geochemical heterogeneities were considered. The upstream weighted multiple cell balance method was employed to numerically solve the governing equations of groundwater flow and virus transport. Model predictions show that the presence of subsurface layered geochemical and physical heterogeneity results in preferential flow paths and thus significantly affect virus mobility. Random distributions of physical and geochemical heterogeneity have also notable influence on the virus transport behavior. While the solution inactivation rate was found to significantly influence the virus transport behavior, surface inactivation under realistic field conditions has probably a negligible influence on the overall virus transport. It was further demonstrated that large virus release rates result in extended periods of virus breakthrough over significant distances downstream from the injection sites. This behavior suggests that simpler models that account for virus adsorption through a retardation factor may yield a

* Corresponding author. Tel.: +1-203-432-2789; fax: +1-203-432-2881.

E-mail address: menachem.elimelech@yale.edu (M. Elimelech).

[1] Current address: Department of Mechanical Engineering, University of Alberta, Edmonton, AB T6G 2G8, Canada.

[2] Department of Civil, Architectural, and Environmental Engineering, University of Colorado, Boulder, CO 80309, USA.

PII: S0169-7722(02)00007-4

misleading assessment of virus transport in ''hydrogeologically sensitive'' subsurface environments.

Keywords: Virus transport; Modeling virus transport; Virus inactivation; Surface inactivation; Geochemical heterogeneity; Physical heterogeneity; Groundwater

1. Introduction

Concern about pathogenic microbes in groundwater has led the US Environmental Protection Agency (2000) to propose the Ground Water Rule, a measure aimed at establishing criteria for the disinfection of drinking water supplies originating from groundwater. Historically, groundwater has been assumed to be free of pathogenic viruses, bacteria, and protozoa, but recent surveys indicate that a significant fraction of groundwater supplies are a source of water-borne diseases (Abbaszadegan et al., 1999). Provisions of the Ground Water Rule include assessments of the ''hydrogeological sensitivity'' of aquifers to the transport of pathogenic microbes. If at least four orders of magnitude reduction in virus concentration cannot be achieved between a potential virus source (e.g., septic tank, leaking sewer line, or sewage infiltration beds) and a water supply well, the aquifer will be considered *hydrogeologically sensitive*. For such aquifers, stringent source water monitoring and disinfection requirements will be imposed.

The EPA designated viruses as the target microbe for the Ground Water Rule because viruses are responsible for most outbreaks of water-borne disease (US Environmental Protection Agency, 2000). Several sensitive aquifer settings are identified in the Ground Water Rule—fractured rock, karst, gravel, and possibly sandy aquifers—based mainly on the rate of groundwater flow through such aquifers. Reduction of virus concentration in aquifer transport occurs by attachment of viruses to aquifer surfaces (so-called deposition) and inactivation of viruses (Schijven and Hassanizadeh, 2000). By incorporating these processes into groundwater transport models, predictions of virus removal in aquifers can be made to aid in the classification of hydrogeologic sensitivity.

Virus attachment is dominated by electrostatic interactions between virus and aquifer grain surfaces (Gerba, 1984; Bitton and Harvey, 1992). If virus and grain surface charges are known, virus attachment behavior can be predicted, at least qualitatively, using classic DLVO theory (Derjaguin and Landau, 1941; Verwey and Overbeek, 1948). Conditions that reduce the electrostatic repulsion between viruses and grains, like low pH, presence of divalent cations, and high ionic strength, favor attachment (Zerda et al., 1985; Penrod et al., 1996). Because most viruses are negatively charged at typical groundwater pH, attachment is also promoted by the presence of positively charged minerals on stationary solid matrix (e.g., iron oxyhydroxides) (Murray and Parks, 1980; Taylor et al., 1981; Loveland et al., 1996; Ryan et al., 1999).

Over the past 20 years, models of virus transport in saturated porous media have portrayed attachment in different ways. Attachment was first modeled as equilibrium sorption with a distribution coefficient (K_d) and retardation (Vilker and Burge, 1980; Yates et al., 1987). VIRALT (Park et al., 1992), a virus transport model commissioned by the US Environmental Protection Agency (EPA), used equilibrium sorption to account for virus

attachment. VIRALT was not successful in predicting virus transport in case studies (Yates, 1995). Much of the poor performance of VIRALT was attributed to the sensitivity of model predictions to the virus distribution coefficient, a poorly known parameter. In addition, more detailed studies of virus transport showing unretarded breakthrough and slow, non-equilibrium release persuaded researchers that virus attachment was not governed solely by equilibrium sorption (Bales et al., 1991). To account for these aspects of virus transport behavior, Bales et al. (1991) introduced a two-site virus attachment model incorporating sites with reversible equilibrium sorption and sites with kinetically controlled attachment and release. Equilibrium sorption was used to characterize the weak attachment of viruses, which are probably deposited in shallow energy minima of the virus–solid surface interaction energy profile. The kinetic attachment rate coefficient was related to the colloid filtration parameters of collision efficiency and single collector efficiency (Yao et al., 1971; Rajagopalan and Tien, 1976). The kinetic release rate coefficient was usually much smaller than the attachment rate coefficient. This two-site approach was adopted in EPA's second-generation virus transport model, CANVAS (Park et al., 1993). Recent efforts have achieved adequate characterization of virus transport with a single-site kinetic attachment and release model (Dowd et al., 1998; Rehmann et al., 1999; Schijven et al., 1999).

Virus inactivation is affected by temperature, solution composition and pH, and attachment (Yates et al., 1987), but only the effect of temperature on the inactivation of viruses in solution was incorporated in the CANVAS model. Attachment appears to play an important role in virus inactivation, but the effect of attachment on surface inactivation is not clear. In the presence of disinfectants, attachment inhibits virus inactivation (Stagg et al., 1977; Liew and Gerba, 1980); but without disinfectants present, attachment to mineral surfaces generally accelerates inactivation (Murray and Parks, 1980). The extent of attachment-accelerated inactivation depends on the strength of attachment of the virus to the mineral surface and the virus type (Schijven and Hassanizadeh, 2000). Recent models of virus transport have incorporated inactivation of attached viruses (Chrysikopoulos and Sim, 1996; Rehmann et al., 1999; Schijven et al., 1999), but the rate coefficient for inactivation of attached viruses is a relatively unknown parameter.

A widely ignored aspect of virus transport is the physical and geochemical heterogeneity of aquifers. Most of the models discussed above deal solely with homogeneous porous media; only Rehmann et al. (1999) has considered the effects of spatial variability of hydraulic conductivity and virus transport parameters. The importance of geochemical heterogeneity has been investigated in colloid transport (Johnson et al., 1996; Elimelech et al., 2000; Ren et al., 2000), but not yet applied to virus transport modeling. Additionally, the dynamics of colloid attachment have been extensively studied (Song and Elimelech, 1993, 1994; Johnson and Elimelech, 1995; Ko et al., 2000), but not yet applied to virus transport modeling. Progressive deposition of colloids on grain surfaces alters the rate of attachment, resulting in either inhibition (blocking) or enhancement (ripening) of further colloid attachment (Kuhnen et al., 2000). A typical virus contamination source in groundwater is expected to release viruses for a long time; therefore, the dynamics of virus attachment may be important.

The present study is aimed at the development of a two-dimensional transport model for predicting virus transport in heterogeneous subsurface porous media such as groundwater aquifers. The model incorporates (1) geochemical (surface charge) heterogeneity of aquifer

grains, (2) physical heterogeneity (pertaining to variations in hydraulic conductivity) of the aquifer, (3) dynamic (transient) aspects of virus attachment and release, and (4) virus inactivation in solution and on aquifer grain surfaces. Simulations of virus transport in a model subsurface environment were performed using this approach to predict the influence of various model parameters on the identification of hydrogeologically sensitive aquifers.

2. Governing equations for virus transport

In this section, we outline the mathematical model for two-dimensional virus transport in a physically and geochemically heterogeneous porous medium. The modeling approach has been described in considerable detail elsewhere (Sun et al., 2001) where it was developed to address colloid transport. This section delineates some of the key features of the model and certain modifications that address various additional mechanisms pertinent to virus transport, specifically, modified models for virus attachment to and release from the collector grains incorporating the effects of virus inactivation on the solid matrix surfaces, and inactivation of the viruses in the solution.

2.1. Virus transport equation

Virus transport in porous media may be described by the advection–dispersion equation along with appropriate terms considering virus attachment, release, and inactivation:

$$\frac{\partial n}{\partial t} = \nabla \cdot (\overline{\mathbf{D}} \cdot \nabla n) - \nabla \cdot (\mathbf{V} n) - R_a - k_i n. \tag{2.1}$$

Here, n is the virus number concentration in the dispersed (solution) phase, t is the time, $\overline{\mathbf{D}}$ is the dispersion tensor, $\mathbf{V}$ is the interstitial fluid velocity, and k_i is the inactivation rate constant of viruses in the dispersed (solution) phase. The source/sink term R_a comprises rate expressions governing virus attachment, release, and surface inactivation and will be described in the next subsection.

The components of the hydrodynamic dispersion tensor, $\overline{\mathbf{D}}$, for a two-dimensional system are given by (Sun, 1995)

$$D_{ij} = \alpha_L \overline{V} \delta_{ij} + (\alpha_L - \alpha_T) \frac{\overline{V}_i \overline{V}_j}{\overline{V}} + D_\infty \delta_{ij} \tag{2.2}$$

where $\overline{V}$ is the average interstitial velocity in the porous medium, $\overline{V}_i$ and $\overline{V}_j$ are the components of the interstitial velocity along the two coordinate directions, α_L and α_T are the longitudinal and transverse dispersivities, respectively, D_∞ is the virus diffusion coefficient, and δ_{ij} is the Kronecker delta.

The interstitial fluid velocity components are determined from the subsurface flow equation and Darcy's law (Sun, 1995). The transient flow equation for a fluid in a subsurface porous medium is represented by (Bear, 1988)

$$S_s \frac{\partial h}{\partial t} = \nabla \cdot (\overline{\mathbf{K}} \cdot \nabla h) - Q. \tag{2.3}$$

Here, h is the hydraulic head, S_s is the specific storage, $\overline{\mathbf{K}}$ is the hydraulic conductivity, and Q is a source/sink term describing pumping or recharge rates. Under natural gradient flow conditions, the steady-state form of the above equation describes the spatial distribution of the hydraulic heads, which are, in turn, used to determine the velocity field employing Darcy's law:

$$\mathbf{q} = -\overline{\mathbf{K}} \cdot \nabla h \tag{2.4}$$

where $\mathbf{q}$ is the Darcy velocity. The mean interstitial velocity, V, is the ratio of the Darcy velocity to the porosity of the medium.

This generalized set of governing equations forms the basis of the virus transport model. This study focuses on a two-dimensional transport in a saturated aquifer, which may contain layered or random spatial variations of physical heterogeneity leading to spatial distributions of the hydraulic conductivity. Furthermore, our goal is to incorporate geochemical heterogeneity of the subsurface porous medium (due to metal oxyhydroxide coatings of matrix grains) that can lead to spatially distributed virus removal rates. The spatial variation of the virus removal rates stems from the different rates of virus attachment, release, and surface inactivation in the geochemically heterogeneous subsurface porous medium.

2.2. Rate of surface coverage

The mechanism for the removal of viruses from the solution phase due to attachment to the stationary phase (collector grains) and the corresponding evolution of virus concentration in the stationary phase may be expressed by

$$\mathrm{V_S} \underset{k_r}{\overset{k_a}{\rightleftharpoons}} \mathrm{V_A} \overset{k_{i,s}}{\rightarrow} \mathrm{V_I}. \tag{2.5}$$

In this kinetic relationship, $\mathrm{V_S}$ denotes virus in the solution, $\mathrm{V_A}$ represents virus in the stationary solid matrix, and $\mathrm{V_I}$ represents the inactive virus. The rate constants k_a, k_r, and $k_{i,s}$ pertain to the rates of attachment, release, and surface inactivation, respectively.

On the basis of the above mechanism, the removal rate of viruses from the solution phase ($\mathrm{V_S}$) due to deposition (attachment) and release can be written as

$$-R_a = -f[k_a B(\theta) n - k_r C_A]. \tag{2.6}$$

In Eq. (2.6), f is the specific surface area of the collector media (i.e., available surface area per unit volume) (Johnson and Elimelech, 1995), $B(\theta)$ is the dynamic blocking function, θ is the fractional surface coverage, which is defined as the fraction of the available surface area occupied by the attached viruses, and C_A is the surface concentration of the attached viruses (number per unit area). The corresponding rate expression for the surface concentration of the attached viruses ($\mathrm{V_A}$) is

$$\frac{\mathrm{d}C_A}{\mathrm{d}t} = k_a B(\theta) n - k_r C_A - k_{i,s} C_A \tag{2.7}$$

with the last term representing the rate of surface inactivation.

Assuming the viruses to be spherical particles of radius a_p, the surface concentrations can be converted to the fractional surface coverage θ. There are, however, two distinct ways in which the fractional surface coverage may be calculated depending on the fate of the inactive viruses. For convenience, we will denote these pathways as M1 and M2. First, the inactivation of attached viruses may result in disintegration and release of the virus components (protein capsid and nucleic acid) from the surface. The release of the virus components does not affect the virus concentration in solution, but it does allow further attachment of intact viruses at these attachment sites. This mechanism (M1) is motivated by the research of Murray and Parks (1980), who used radiolabels incorporated in poliovirus capsid and RNA to track the fate of these components following attachment. In this case, the total surface coverage is solely attributed to the active (attached) viruses, and Eq. (2.7) can be written as

$$\frac{d\theta}{dt} = \pi a_p^2 k_a B(\theta) n - k_r \theta - k_{i,s} \theta. \tag{2.8}$$

For the second mechanism (M2), inactivated viruses remain attached to the surface, block further attachment of viruses, and reduce the release of viruses. This mechanism is motivated by field research on the transport of radiolabeled bacteriophage PRD1 in a geochemically heterogeneous aquifer on Cape Cod (Pieper, 1995). Similar mechanisms of surface inactivation in batch systems were proposed by Grant et al. (1993). In this case, the rate of surface coverage may be represented as

$$\frac{d\theta}{dt} = \pi a_p^2 k_a B(\theta) n - k_r [1 - \Phi(t)] \theta. \tag{2.9}$$

The term $\Phi(t)$ in Eq. (2.9) represents the fraction of attached viruses that have undergone surface inactivation.

The dynamic blocking function in the above equations can be expressed in terms of the random sequential adsorption (RSA) model (Ko et al., 2000)

$$B(\theta) = 1 - a_1 \theta + a_2 \theta^2 + a_3 \theta^3 + \cdots \tag{2.10}$$

with appropriate values of the virial coefficients a_i (Ko et al., 2000). It should be noted that the more common Langmuirian adsorption model (Kuhnen et al., 2000) can also be employed to account for the blocking behavior, in which case, Eq. (2.10) is truncated after the first-order term.

Finally, Eq. (2.6) may be recast in terms of the fractional surface coverage as

$$-R_a = -\frac{f}{\pi a_p^2} \left[\pi a_p^2 k_a B(\theta) n - k_r \theta \right] \tag{2.11a}$$

or

$$-R_a = -\frac{f}{\pi a_p^2} \left\{ \pi a_p^2 k_a B(\theta) n - k_r \left[1 - \Phi(t) \right] \theta \right\} \tag{2.11b}$$

for inactivation models M1 and M2, respectively, depending on whether the inactive viruses disintegrate or remain attached to the surface. Note that Eqs. (2.11a) or (2.11b) will

appear in the virus transport equation (Eq. (2.1)), while the time evolution of the surface coverage needs to be determined from either Eq. (2.8) or Eq. (2.9).

2.3. Physical and geochemical heterogeneity

Physical heterogeneity of a porous medium is primarily an outcome of structured or random distributions of hydraulic conductivity throughout the aquifer. In this study, we consider two types of physical heterogeneity: layered heterogeneity and random heterogeneity. In a layered, physically heterogeneous porous medium, the medium is made up of several homogeneous layers. While each layer in such porous media is homogeneous (i.e., with constant hydraulic conductivity), the entire system is heterogeneous. Porous media with fractures (Ibaraki and Sudicky, 1995a,b), large blocks of macropores, or various sedimentary deposits may be described as layered heterogeneous. Random heterogeneity involves continuous spatial distribution of hydraulic conductivity in the aquifer. A log-normal distribution of hydraulic conductivity is generally used in contaminant hydrology (e.g., Dagan, 1989; Gelhar and Axness, 1983; Rubin, 1990), and in this study, we use this distribution to model random physical heterogeneity.

A patchwise surface charge model (Song and Elimelech, 1993; Song et al., 1994; Johnson et al., 1996) is used to describe the geochemical heterogeneity of aquifer grains. Johnson et al. (1996) showed that this model is adequate to describe the heterogeneity resulting from ferric oxyhydroxide patches on grain surfaces, a typical form of surface charge heterogeneity that has a significant effect on the transport of microbes (Scholl and Harvey, 1992; Knapp et al., 1998; Ryan et al., 1999; Schijven et al., 2000). With this model, the surface coverage θ is represented as a linear combination of the fractional coverage pertaining to favorable patches and unfavorable surfaces, i.e., (Johnson et al., 1996)

$$\theta = \lambda\theta_{\mathrm{f}} + (1-\lambda)\theta_{\mathrm{u}} \tag{2.12}$$

where λ is the heterogeneity parameter describing the fraction of aquifer grains coated with favorable attachment patches, and θ_{f} and θ_{u} are the favorable and unfavorable aquifer solid matrix surface fractions, respectively. For viruses, most of which are negatively charged at typical groundwater pH (6–8), favorable attachment sites are positively charged (e.g., iron and aluminum oxides, edges of clay minerals). In the iron oxyhydroxide-coated sand aquifer on Cape Cod, Massachusetts, λ is about 3–4% (Ryan et al., 1999). The spatial distribution of the heterogeneity parameter λ in the aquifer bed can either be layered or random as in the case of physical heterogeneity.

Using the patchwise model, the rate expression for surface coverage by retained viruses is given by (Johnson et al., 1996)

$$\frac{\partial\theta}{\partial t} = \lambda\frac{\partial\theta_{\mathrm{f}}}{\partial t} + (1-\lambda)\frac{\partial\theta_{\mathrm{u}}}{\partial t} \tag{2.13}$$

The dynamics of deposition on the favorable fraction of the aquifer grains can now be written explicitly for the two modes of surface inactivation M1 or M2 as

$$\frac{\partial\theta_{\mathrm{f}}}{\partial t} = \pi a_{\mathrm{p}}^2 k_{\mathrm{a,f}} nB(\theta_{\mathrm{f}}) - k_{\mathrm{r,f}}\theta_{\mathrm{f}} - k_{\mathrm{i,s,f}}\theta_{\mathrm{f}} \tag{2.14a}$$

or

$$\frac{\partial \theta_f}{\partial t} = \pi a_p^2 k_{a,f} n B(\theta_f) - k_{r,f}[1 - \Phi_f(t)]\theta_f \tag{2.14b}$$

respectively. Similarly, for the unfavorable fraction of the aquifer grains, the corresponding rate expressions will be

$$\frac{\partial \theta_u}{\partial t} = \pi a_p^2 k_{a,u} n B(\theta_u) - k_{r,u}\theta_u - k_{i,s,u}\theta_u \tag{2.15a}$$

or

$$\frac{\partial \theta_u}{\partial t} = \pi a_p^2 k_{a,u} n B(\theta_u) - k_{r,u}[1 - \Phi_u(t)]\theta_u \tag{2.15b}$$

where the subscripts f and u refer to the favorable and unfavorable surfaces, respectively. Because colloid and virus attachment to favorable (oppositely charged) patches (e.g., ferric oxyhydroxide coatings) is in a deep primary minimum of the interaction energy profile (Johnson et al., 1996; Loveland et al., 1996), spontaneous release from favorable patches can be neglected, barring changes in solution chemistry.

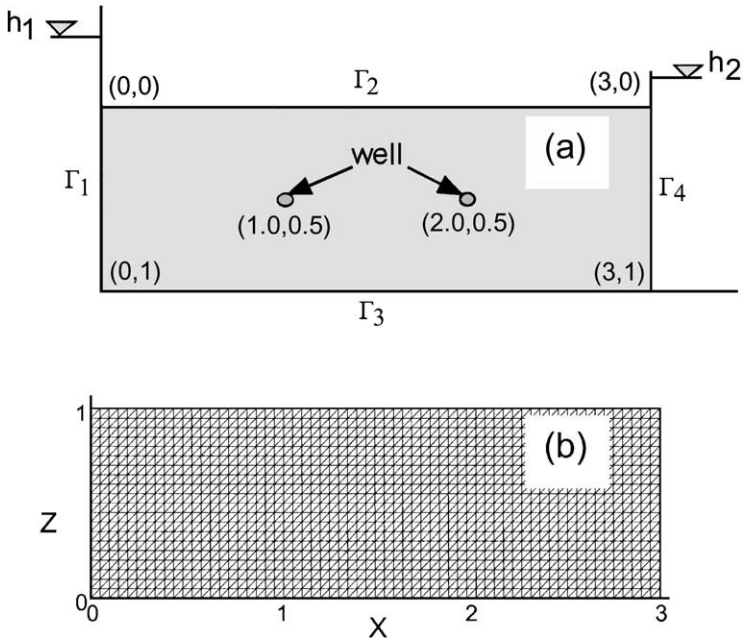

Fig. 1. Schematic representation of (a) the two-dimensional computational domain, and (b) the finite element mesh used to discretize the domain. The flow is along the horizontal (x) direction. In all the simulations, the virus particles are injected along the left boundary (Γ_1). Wells can be located at any position in the domain (two shown).

3. Model system and numerical methods

The coupled groundwater flow and virus transport equations were solved numerically for both transient and steady state flow fields using the multiple cell balance (MCB) method (Sun et al., 2001; Sun, 1995). In this section, we briefly describe the model system used in the simulations, including the domain geometry, various initial and boundary conditions, model parameters, and the numerical technique used for the solution of the governing transport equations.

3.1. Initial and boundary conditions

We consider a 3-m long and 1-m deep rectangular domain ($\Omega(x,z)$, where $0 \le x \le 3$, and $0 \le z \le 1$) for the simulations (Fig. 1). The four-line boundaries of the rectangular computational domain are also depicted in the figure (Γ_1 on which $x=0$, Γ_2 on which $z=0$, Γ_3 on which $z=1$, and Γ_4 on which $x=3$). The initial and boundary conditions for the flow equation at these boundaries are specified as follows:

$$h(x) = h_0 \quad \text{at} \quad t = 0, \tag{3.1a}$$

$$h(0,z,t) = h_1 \quad \text{for} \quad t > 0,\ (0,z) \in \Gamma_1, \tag{3.1b}$$

$$\frac{\partial h(x,z,t)}{\partial z}\Big|_{z=0} = 0 \quad \text{for} \quad t > 0,\ (x,0) \in \Gamma_2, \tag{3.1c}$$

$$\frac{\partial h(x,z,t)}{\partial z}\Big|_{z=1} = 0 \quad \text{for} \quad t > 0,\ (x,1) \in \Gamma_3, \tag{3.1d}$$

$$h(3,z,t) = h_2 \quad \text{for} \quad t > 0,\ (3,z) \in \Gamma_4, \tag{3.1e}$$

where h_1 and h_2 are fixed values of hydraulic heads on the boundaries. The steady-state flow field is generated by using the transient flow equation, Eq. (2.3), for sufficiently long time.

The initial and boundary conditions for the virus transport equation are specified according to the methods of virus injection. Initially the porous medium has no virus particles (i.e., zero concentration everywhere in the domain and zero surface coverage, $\theta_f = \theta_u = 0$). At the four boundaries of the rectangular domain (Γ_1, Γ_2, Γ_3, and Γ_4), zero dispersive flux boundary conditions are specified. At a given time $t > 0$, the virus injection is initiated at a fixed concentration and rate at specified locations in the domain. The injection is modeled as a step function which can be switched on at time $t = t_0$ and switched off at time $t = t_1$ where $t_1 > t_0$. Depending on the magnitude of $(t_1 - t_0)$, the type of virus injection can be classified as pulse injection ($t_1 \approx t_0$) or continuous injection ($t_1 \gg t_0$). The mode of injection can be characterized as point injection or line injection based on the number and locations of injection wells. The injection is set as the boundary condition for the virus concentration.

Table 1
Hydrologic and transport parameters used in the model simulations

Parameter	Value	Comments
Hydrologic		
Head gradient, ∇h	0.01	10^{-4}–10^{-1}
Initial head, h_0	20 m	
Conductivity, K	100 m day^{-1}	1–1000
Storage, S_s	0.0001	
Dispersivity (longitudinal), α_L	0.05 m	0.01–0.07
Dispersivity (transverse), α_T	0.005 m	$\alpha_L/\alpha_T \sim 5$–20
Porosity, ε	0.4	0.3–0.5
Transport		
Collector diameter, d_c	3.0×10^{-4} m	
Virus diameter, d_p	6.0×10^{-8} m	Generally 20–200 nm
Specific surface area, f	3.0×10^{4} m^{-1}	Using $6(1-\varepsilon)/(\varepsilon d_c)$
Inlet virus concentration, n_0	1.0×10^{11} m^{-3}	10^{8}–10^{14}
Favorable surface fraction, λ	0.01 (1%)	0–0.1
Collision efficiencies/rate constants		
Deposition (favorable), α_f	1.0	
Deposition (unfavorable), α_u	0.005	0.001–0.01
Release (favorable), $k_{r,f}$	0	No detachment from favorable fraction
Release (unfavorable), $k_{r,u}$	1.0×10^{-4} day^{-1}	1.0×10^{-5}–5.0×10^{-1} day^{-1}
Inactivation (solution), k_i	1.4 day^{-1}	0.29–2.2 day^{-1}

3.2. Model parameters

Table 1 shows the baseline hydrologic and physico-chemical transport parameters used in the computations. The ranges of these parameters, typically encountered in surficial sandy aquifers (Sun et al., 2001), are also shown in the table. All the simulations were performed using parameter values that lie within the specified ranges. Even when performing the calculations in a randomly heterogeneous porous medium, the physical and geochemical heterogeneity distributions were determined such that the specified ranges of these heterogeneities were never exceeded.

The numerical code employs locally defined deposition rate constants, which are evaluated on the basis of the local flow velocities in the porous medium. The deposition rate constant was calculated assuming a Happel flow field (Happel, 1958) around the collector grains in each finite element. The interstitial velocity $V=(V_i^2+V_j^2)^{1/2}$ in each element was used to calculate the single collector efficiency employing the relationship (Elimelech et al., 1995)

$$\eta_0 = 4A_s^{1/3}\left(\frac{D_\infty}{2a_c\varepsilon V}\right)^{2/3} \tag{3.2}$$

where A_s is a constant obtained from Happel's cell model (Happel, 1958), D_∞ is the particle (virus) diffusivity, a_c is the collector grain radius, and ε is the bed porosity. The deposition rate constant is then determined from the single collector efficiency using

$$k_a = \frac{\alpha\eta_0\varepsilon V}{4} \tag{3.3}$$

where the term α, usually referred to as the collision (attachment) efficiency (Elimelech et al., 1995), accounts for the influence of solution chemistry and the chemical nature of the surfaces on virus deposition. The above formulation directly incorporates the influence of the flow field on virus deposition rates, assuming that the deposition of small viruses is not affected by interception or gravity. The model, however, requires independent information about the collision efficiency, which has been chosen as $\alpha_u = 10^{-3} - 10^{-2}$ for the unfavorable surface fraction and $\alpha_f = 1$ for the favorable surface fraction. It should be noted that the deposition rate constant in Eq. (3.3), and throughout this study, has units of m day^{-1}. In most studies on virus transport, the deposition rate constant is generally represented in units of day^{-1} (Rehmann et al., 1999; Schijven et al., 1999; Schijven and Hassanizadeh, 2000). The k_a in the present work, when multiplied by the specific area of the collectors f, will be identical to the deposition rate constants used in such studies.

Literature data show that solution phase (bulk) inactivation rate constants of viruses range between 0.01 and 2 day^{-1} (Tim and Mostaghimi, 1991; Yates, 1995; Schijven and Hassanizadeh, 2000). The solution-phase virus inactivation rate constant was set at $k_i = 1.4$ day^{-1}, a value determined for a temperature of 15 °C using the inactivation rate constant-temperature regression determined for coliphage MS2 by Yates et al. (1985). For surface inactivation, rate coefficients of $k_{i,s,f} = 12$ day^{-1} and $k_{i,s,u} = 0$ day^{-1} were chosen based on bacteriophage PRD1 inactivation rates in the presence of ferric oxyhydroxide-coated sands from the Cape Cod, Massachusetts, field site (Navigato, 1999) and poliovirus inactivation rates on silica surfaces (Murray and Labland, 1979). The virus release rate constants are assumed to be representative of viruses and colloidal particles of similar size (e.g., Rehmann et al., 1999; Sun et al., 2001). Furthermore, assuming that viruses will be captured irreversibly on the favorable surface sites, the corresponding release rate coefficient was always set to zero. Consequently, virus release only from unfavorable surface sites was considered in this study.

3.3. Numerical solution of the governing equations

The coupled groundwater flow and virus transport equations, involving all the mechanisms of virus deposition, release, inactivation, as well as physical and chemical heterogeneities of the porous medium, cannot be solved analytically. These equations were solved numerically using the multiple cell balance (MCB) technique, an adaptation of the finite element method (Sun et al., 2001; Sun, 1995; Sun and Yeh, 1983). The numerical solution was performed using a mesh of linear triangular elements. The primary feature of the computational technique is to ensure that the integral form of Eq. (2.1) or Eq. (2.3) is satisfied for each element as well as over an exclusive subdomain surrounding each node (Sun, 1995). After considering the initial and boundary conditions, we obtain a set of governing ordinary differential equations (ODE) at each node for the time evolution of the hydraulic head or the virus concentration. Solution of the coupled set of ODEs provides the hydraulic head distribution, virus concentration distribution, and the fractional surface coverage over the computational domain.

The system of ODEs was solved numerically using the backward Euler method. Because the transport equation and the surface coverage rate equation are coupled, an iterative scheme was employed to solve these simultaneously. First, the unknown virus bulk con-

centration was calculated on the basis of the surface coverage at the old time level. Then the new surface coverage rate was obtained according to the calculated virus concentration. The surface coverage can be calculated from the surface coverage rate by applying a first-order finite difference scheme

$$\theta_{\mathrm{i}}^{\mathrm{new}} = \theta_{\mathrm{i}}^{\mathrm{old}} + \frac{\partial \theta_{\mathrm{i}}}{\partial t}\Delta t \tag{3.4}$$

where i represents the subscripts f or u corresponding to the favorable and unfavorable surface fractions, respectively, and Δt is the time step. The surface coverage rate is determined from Eqs. (2.9)–(2.11b). The virus concentration and the fractional surface coverage at each node were iteratively updated until a convergence criterion for each of these was satisfied at every node of the domain.

The computations were mostly performed using a finite element mesh comprising 2480 linear triangular elements and 1323 nodes (Fig. 1b). The optimal mesh resolution was determined by starting from a smaller number of nodes and doubling the number of nodes until the concentration profiles from two consecutive meshes were found to be within a few percent (1–6%). To obtain an accurate numerical solution, both numerical dispersion and oscillations were controlled simultaneously in the numerical code. The local mesh Peclet number $\Delta x V/D$, where Δx is the step size along the flow direction, was set to less than 1 to control numerical dispersion. When the fluid velocity was too high, the upstream weighting scheme was included in the MCB code through a weighting parameter to minimize oscillation errors. The Courant number, defined as $V\Delta t/\Delta x$, was also set to less than 1 so that the average displacement of fluid was less than the length of one grid space over each time step.

4. Results and discussion

Results obtained from the solution of the virus transport equations comprise the time evolution of the virus concentration profiles, virus breakthrough information at any location in the model aquifer, and the time evolution of the fractional surface coverage of attached viruses at every location in the domain. In the following, we present some of the simulation results that highlight the capabilities of the model and provide some insight regarding the virus transport mechanisms in various types of aquifer beds.

4.1. Virus concentration profiles in layered heterogeneous porous media

Virus concentration profiles were obtained for a continuous line injection along the boundary Γ_1 into the rectangular model aquifer (Fig. 1). The injection was started at $t = 0.01$ day. In all cases, the virus number concentration in the injected sample was 1×10^{11} m^{-3}. The subsequent virus concentration profiles at the end of the fifth day in the aquifer are shown in Fig. 2. The aquifer bed has been ascribed different physical and chemical heterogeneity to observe the effects of these heterogeneities on the transport behavior. Fig. 2a shows the virus concentration profiles in a homogeneous porous medium with uniform physical heterogeneity (hydraulic conductivity) and a uniformly distributed geo-

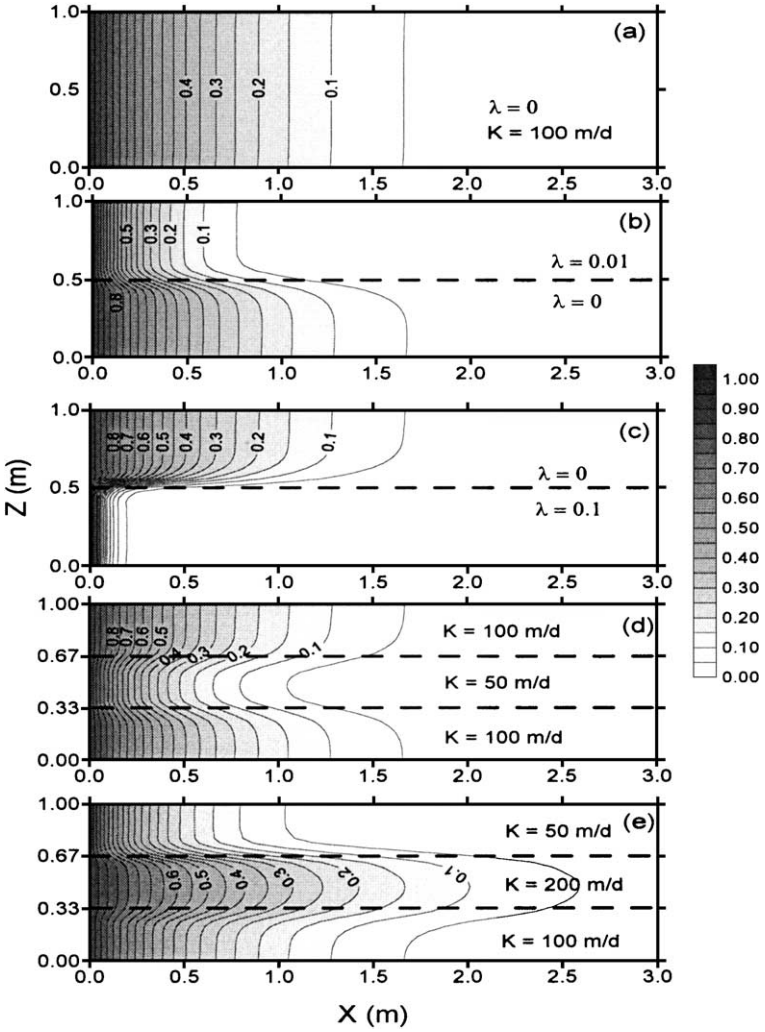

Fig. 2. Virus concentration profiles at $t=5$ days for a continuous line injection at the left boundary for different combinations of layered physical (K) and geochemical (λ) heterogeneity. The injection was initiated at 0.01 day. (a) Hydrogeologically uniform aquifer with $K=100$ m day^{-1} and $\lambda=0$. (b) Uniform hydraulic conductivity with $K=100$ m day^{-1} but in presence of two horizontal layers of geochemical heterogeneity, with $\lambda=0.01$ in the upper half and $\lambda=0$ in the lower half of the domain. (c) Same hydraulic conductivity field as (b), but with $\lambda=0$ in the upper half and $\lambda=0.1$ in the lower half of the domain. (d) Layered hydraulic conductivity field as shown, but a uniform geochemical heterogeneity field of $\lambda=0.01$. (e) Layered hydraulic conductivity field as shown but a uniform geochemical heterogeneity field of $\lambda=0$. The other various parameters used in the simulations are shown in Table 1. The contour labels indicate the scaled virus concentration n/n_0.

chemical heterogeneity field that is completely unfavorable (i.e., $\lambda=0$). The subsequent profiles (Fig. 2b–e) are obtained for different combinations of horizontally layered heterogeneity in the medium. Figs. 2b and 2c represent the concentration profiles in an

aquifer with two layers containing different extents of geochemical heterogeneities (the hydraulic conductivity is uniform over the entire domain). Figs. 2d and 2e are obtained for an aquifer comprising three horizontal layers of different hydraulic conductivity (the geochemical heterogeneity is uniform over the entire domain). Layering of both geochemical and physical heterogeneity can result in considerably different mobility of the viruses in the aquifer beds. Such layered heterogeneities can result in preferential flow paths, thus enhancing virus mobility is the subsurface porous medium.

Fig. 3 shows the combined influence of layered geochemical and physical heterogeneity on virus movement in an aquifer. The aquifer shown here consists of three horizontal layers with different combinations of physical and geochemical heterogeneity. The virus concentration profile shown in Fig. 3a was obtained using a hydraulic conductivity of 50 m day^{-1} in the central layer and 200 m day^{-1} in the two adjacent layers, while the geochemical heterogeneities were assigned to be 1% in the central layer and 0% in the two peripheral layers. In Fig. 3b, the concentration profiles are shown with the same distribution of physical heterogeneity, but the geochemical heterogeneities were redistributed by assigning $\lambda = 0$ in the central layer, and $\lambda = 0.01$ (1%) in the peripheral layers. All other conditions were kept constant in the two simulations. The combination of physical and geochemical hetero-

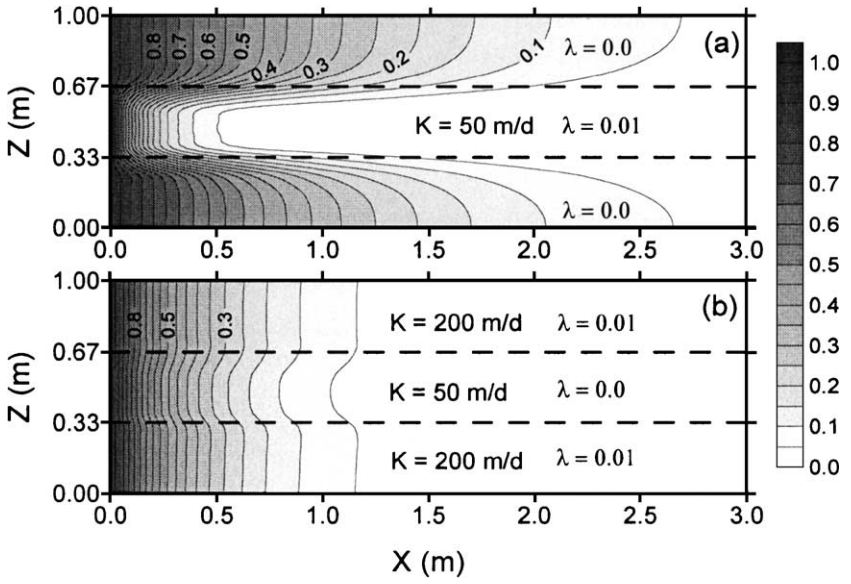

Fig. 3. Relative importance of combined layered physical and geochemical heterogeneity on the movement of viruses in the model aquifer. The virus concentration profile is shown at $t = 5$ days for a domain containing three horizontal layers with different hydrogeological properties. These concentration maps were obtained using the same type of injection employed in Fig. 2 (i.e., continuous line injection at the left boundary). In (a), the middle layer of the domain has $K = 50$ m day^{-1} while the two outer layers have $K = 200$ m day^{-1}; the heterogeneity parameter in the middle layer is $\lambda = 0.01$, while in the two outer layers, $\lambda = 0$. In (b), the hydraulic conductivities of the three layers are same as in (a), but $\lambda = 0$ in the middle layer while $\lambda = 0.01$ in the two outer layers. The other various parameters used in the simulations are shown in Table 1. The contour labels indicate the scaled virus concentration n/n_0.

geneity can result in a significant shift in the movement patterns of the viruses in groundwater aquifers. The results also demonstrate that layered geochemical heterogeneity can significantly alter the preferential transport of viruses caused by layered physical heterogeneity. Hence, consideration of physical or geochemical heterogeneity alone in virus transport models may result in erroneous results.

4.2. Transport in randomly heterogeneous porous media

Although layered heterogeneity models can capture spatial variations of the hydrogeological properties of an aquifer in terms of an effective (mean) property value over a layer, there can be more fine-grained heterogeneity in a natural aquifer that may be distributed randomly within a layer. Such random distribution of hydrogeological properties may be considered in terms of appropriate statistical models. In this study, the hydraulic conductivity (K) and the fraction of favorable surfaces (λ) were modeled using log-normal distributions. With known mean and variance of the distributions, the entire spatial distribution of these parameters in the aquifer can be constructed employing a turning band method (Mantoglou and Wilson, 1982; Tompson et al., 1989; Sun et al., 2001). The covariance function of the distribution is described by an isotropic exponential function of the form (Sun et al., 2001)

$$C_Y(r) = \sigma_Y^2 \exp\left(-\frac{|\mathbf{r}_Y|}{l_Y}\right) \tag{4.1}$$

where Y is the log-normally distributed physical (K) or geochemical (λ) field, $\mathbf{r}_Y$ is the planar distance vector between two positions in the domain, σ_Y^2 is the variance of the distribution (Y), and l_Y is the characteristic correlation length of the distribution. Using statistical properties of the spatial distribution, the random fields for the hydraulic conductivity and the geochemical heterogeneity parameter can be generated.

In Fig. 4, we show the influence of a randomly distributed hydraulic conductivity field on virus transport. The simulations were performed for a geochemically uniform aquifer comprising completely unfavorable collector grains but with a randomly distributed hydraulic conductivity with a mean value of 100 m day^{-1}. We note here that unlike the previous calculations, the present simulations were performed using the unsteady flow equations, since in presence of randomly distributed hydraulic conductivity fields, a steady state head distribution takes a considerably long time to develop. Under such conditions, variations of the hydraulic conductivity would lead to local variations of the velocity field in the aquifer. According to Eqs. (3.2) and (3.3), such variable velocity fields will result in local variations of the deposition rate constant (k_a is proportional to $K^{1/3}$ (Sun et al., 2001)). In Fig. 4, the random K fields, the corresponding head distributions, and the concentration distributions after 5 days are shown for different values of variance (σ_y^2) in the log-normal distributions of K. Figs. 4a–d were obtained corresponding to a mean hydraulic conductivity of 100 m day^{-1} and a correlation distance of 0.5 m (Sun et al., 2001), but for increasing values of the variance; that is, $\sigma_y^2 = 0.0024$ in (a), 0.024 in (b), 0.24 in (c) and 0.74 in (d). It is noted that presence of hydraulic conductivity distribution enhances virus transport (Figs. 4c and 4d). When the hydraulic conductivity field is

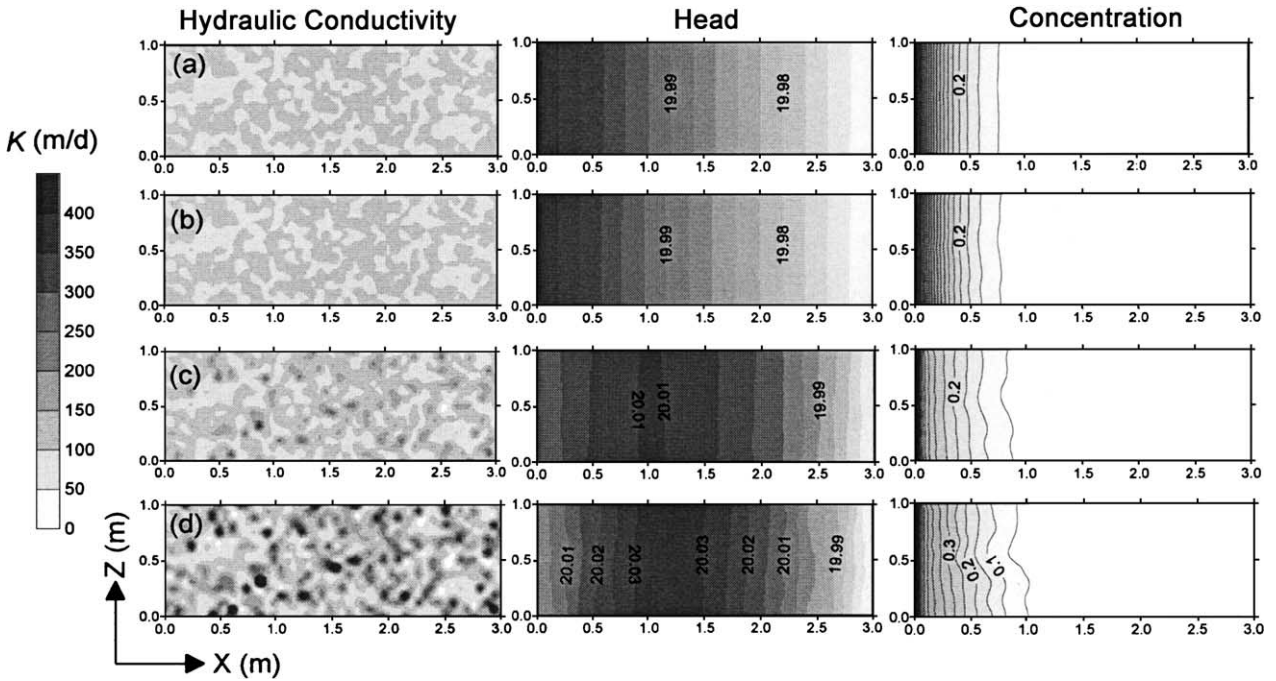

Fig. 4. Influence of randomly distributed physical heterogeneity on virus transport. The simulations were performed for a continuous line injection at the left boundary of a domain containing a geochemically homogeneous ($\lambda = 0$) porous bed. The three maps in each row represent the hydraulic conductivity field, the hydraulic head, and the virus concentration distribution (n/n_0) after 5 days, respectively. In all cases, the hydraulic conductivity field was generated using a mean value of $K = 100$ m day^{-1} and a correlation length of 0.5 m. The variances of the distributions were (a) = 0.0024, (b) = 0.024, (c) = 0.24, and (d) = 0.74. The darker shades in the hydraulic conductivity realization maps (left column) represent domains of high hydraulic conductivity. The other various parameters used in the simulations are shown in Table 1.

changed by increasing the variance to 0.74 (Fig. 4d), we note a marked alteration in the virus concentration distribution. The larger variance in the distribution leads to patches where the conductivity becomes very large (darkest regions in Fig. 4d correspond to K>500 m day^{-1}). We thus note that a randomly heterogeneous hydraulic conductivity field can result in drastic changes in the virus movement, providing preferential pathways for advective and dispersive transport.

An important outcome of large variances in the hydraulic conductivity becomes apparent from the hydraulic head distributions in Figs. 4c and 4d (in the two instances with the largest variances). Here, we note that the transient hydraulic heads become slightly higher at about 1 m downstream from the left boundary. In other words, there appears to be a natural flow barrier developing in this region that prevents the flow of viruses past the 1-m plane. This behavior stems from the presence of extremely low hydraulic conductivity patches just upstream of the 1-m plane. Such regions behave as a natural barrier to the transport of viruses and, as a consequence, the overall virus migration is restricted to about 1-m downstream from the injection plane.

The influence of a randomly distributed geochemical heterogeneity field on the virus transport behavior is shown in Fig. 5. In this case, the simulations were performed assuming a constant hydraulic conductivity (100 m day^{-1}) of the medium, while the geochemical heterogeneity parameter was assumed to be distributed log-normally with a known mean value and variance. Figs. 5a and 5b depict two randomly distributed geochemical fields with a mean favorable attachment surface fraction of 1% (i.e., $\lambda = 0.01$) and a correlation distance of 0.5 m, but with two values of the variance, namely, 0.024 and 0.24. The virus concentration fields under steady flow conditions after five days corresponding to these geochemical heterogeneity distributions are shown in Fig. 5c and 5d, respectively. It is evident that the virus concentration fronts move more slowly when the variance in the heterogeneity distribution becomes larger. We also note that the concentration profiles are highly non-uniform and there is significantly slower virus movement in isolated regions where the favorable surface fractions are present in higher density. Therefore, it might be concluded that presence of random geochemical heterogeneity results in significant "local" alterations in the virus transport behavior. Furthermore, the mean value of the geochemical heterogeneity is important in governing the overall extent of virus infiltration. In light of the fact that log-normal distributions tend to be skewed to yield large λ values, the arithmetic mean geochemical heterogeneity becomes larger when the variance of the log-normal distribution increases. Therefore, the influence of geochemical heterogeneity on virus transport is not only significant locally, but also quite important on the global virus movement behavior in the aquifer.

4.3. Virus breakthrough behavior

Although virus breakthrough behavior can be influenced by all the physical and chemical parameters shown in Table 1, it is of particular interest to explore the extent to which attachment, release, and inactivation terms affect virus transport. In this section, we present simulation results that depict the importance of these terms in governing the virus breakthrough behavior. In the following, all simulations were performed for a constant (uniform) physical and geochemical heterogeneity fields, unless otherwise mentioned.

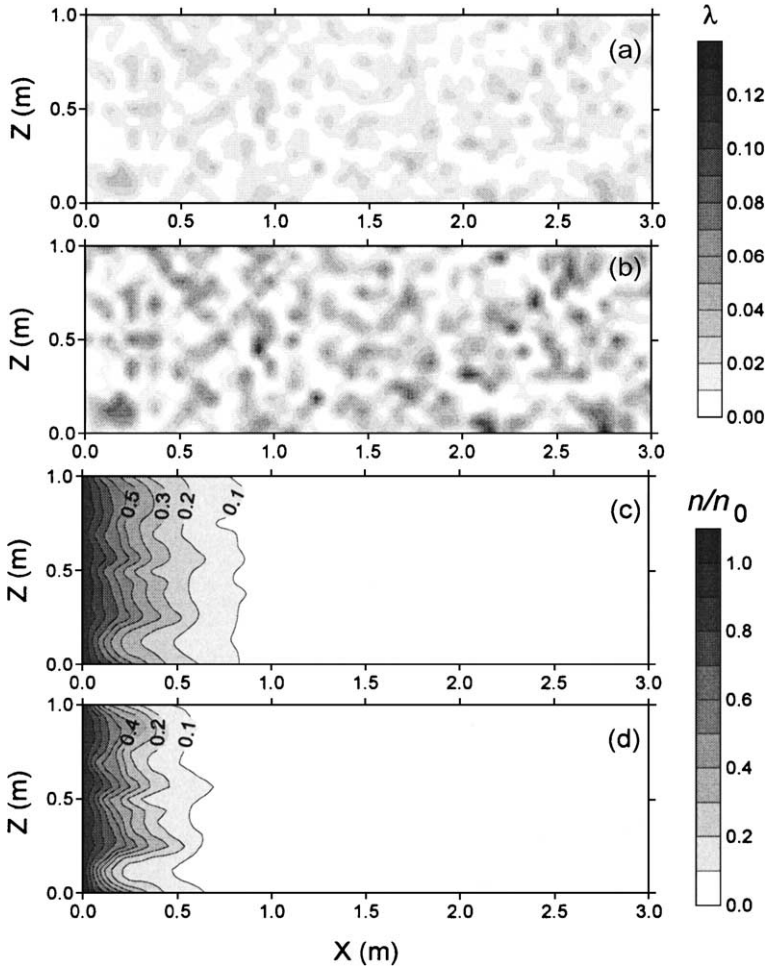

Fig. 5. Influence of randomly distributed geochemical heterogeneity on virus transport. Simulations were performed in a homogeneous hydraulic conductivity field with $K = 100$ m day^{-1} employing a continuous line injection at the left boundary. (a) and (b) show two realizations of the random geochemical heterogeneity field with a mean value of $\lambda = 0.01$ and two different variances, namely, 0.024 and 0.24, respectively. The corresponding virus concentration profiles (n/n_0) after 5 days are shown in (c) and (d), respectively. The other various parameters used in the simulations are shown in Table 1.

4.3.1. Influence of geochemical heterogeneity

The geochemical heterogeneity parameter governs the distribution of favorable and unfavorable patches available for virus deposition. Virus breakthrough behavior at an observation well located 0.5-m downstream from a line injection at the boundary of the aquifer (Fig. 1) is shown in Fig. 6 for different geochemical heterogeneity parameter values. The breakthrough data were obtained for a pulse injection that was initiated at $t = 0.01$ day and terminated after 1 day. It is noted that increasing the fraction of favorable patches

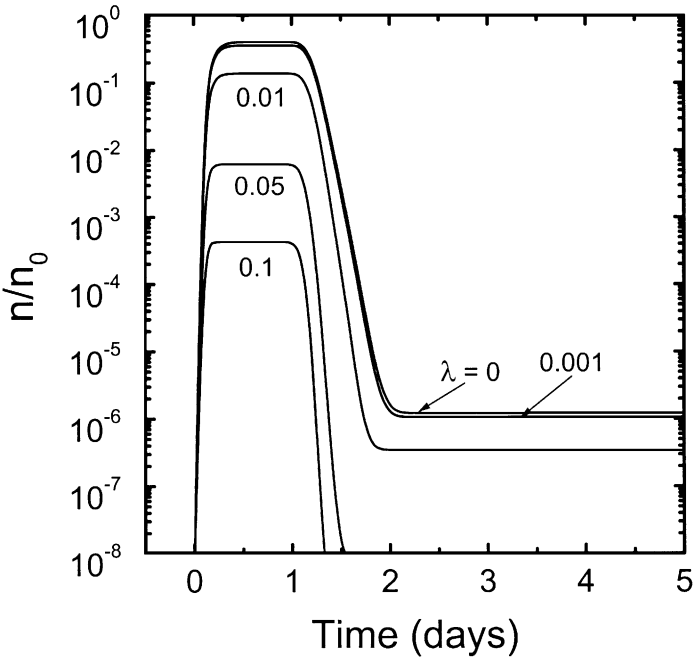

Fig. 6. Virus breakthrough behavior at the observation well located at (0.5, 0.5) corresponding to different mean geochemical heterogeneity (λ) values. The results were obtained for uniform physical and geochemical heterogeneity fields with $K = 100$ m day^{-1}, and the values of λ as indicated. The collision efficiencies (α) for the favorable and unfavorable surface fractions are 1 and 0.005, respectively. Release was considered only from the unfavorable surface fractions, with the release rate coefficient being 10^{-4} day^{-1}. The results were obtained for a pulse line injection at the left boundary of the domain. The injection started at 0.01 day and was stopped at 1 day. The other various parameters used in the simulations are shown in Table 1.

attenuates the virus breakthrough considerably. For a 10% favorable attachment surface fraction ($\lambda = 0.1$) in the aquifer, the virus concentrations at the observation well was found to be almost three orders of magnitude smaller than the inlet concentration at all observation times.

4.3.2. Influence of inactivation in solution

The solution-phase inactivation term in the virus transport model results in a decrease in the concentration of the viruses in solution. Fig. 7 shows the influence of the solution inactivation rate constant on the virus breakthrough. It is evident that variations of the inactivation rate constant are not important as long as $k_i \leq 1.0$ day^{-1}. However, larger values of k_i tend to significantly reduce the peaks of the virus breakthrough profiles as well as the long-term residual virus concentrations at the observation well.

4.3.3. Influence of virus release

Because virus attachment to the oppositely charged favorable surface fraction is in a deep primary minimum (Loveland et al., 1996), the favorable surface release rate coefficient was

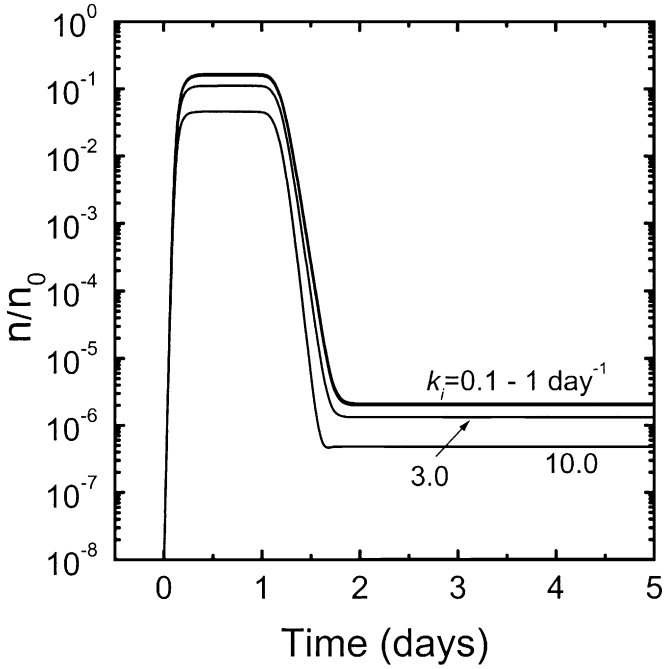

Fig. 7. Influence of the solution phase virus inactivation rate constant, k_i, on virus breakthrough behavior at an observation well located at (0.5, 0.5). The simulations were performed for a hydrogeologically homogeneous aquifer with $K = 100$ m day^{-1} and $\lambda = 0.01$ employing a pulse injection of viruses at the left boundary. The injection started at 0.01 day and was stopped at 1 day. The other various parameters used in the simulations are shown in Table 1.

set to zero. All release occurs from the viruses attached to the unfavorable attachment surfaces. Fig. 8 depicts the influence of the virus release rate constant on the breakthrough behavior at an observation well located 0.5-m downstream from the injection line. Although virus release does not influence the primary peak of the breakthrough curves, the long-term breakthrough behavior registers the influence of the release rate constant. When the release rate constant becomes large, we observe a sustained residual virus concentration (tailing) at the well over a long time period.

4.3.4. Influence of surface inactivation

In Section 2.2, two possible scenarios (M1 and M2) were considered to model the fate of the attached viruses once they undergo surface inactivation. According to mechanism M1, the inactive viruses disintegrate and vacate the surface sites to allow for further attachment of active viruses. In contrast, mechanism M2 suggests that the inactive viruses remain attached to the surface, and consequently, inhibit the deposition rate of the active viruses. For either mechanism, noting that the rate of surface inactivation solely depends on the fractional surface coverage of active viruses at a given time, it is clearly discernable that this term is negligible for low virus deposition rates. Accordingly, some preliminary simulations were performed to determine under which conditions surface inactivation might become

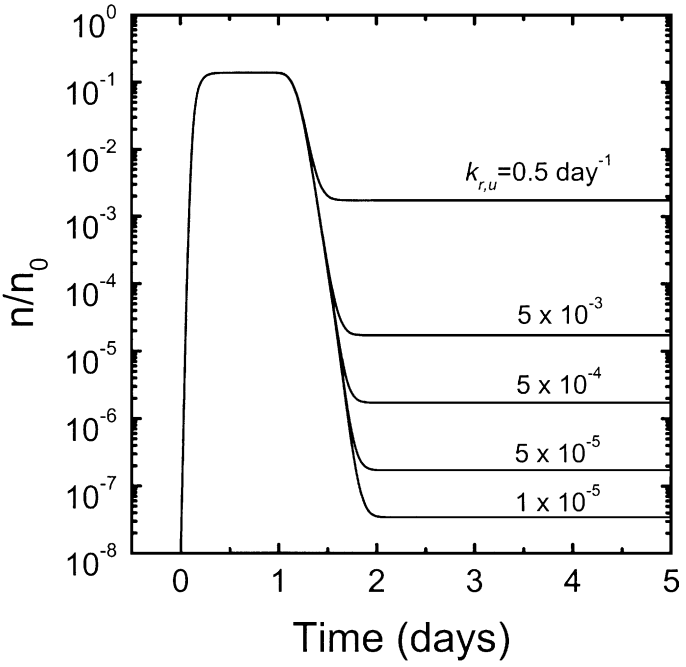

Fig. 8. Influence of virus release rate constant on the breakthrough behavior at an observation well located at (0.5, 0.5). The simulations were performed for a hydrogeologically homogeneous aquifer with $K = 100$ m day^{-1} and $\lambda = 0.01$ employing a pulse injection of viruses at the left boundary. The injection started at 0.01 day and was stopped at 1 day. The other various parameters used in the simulations are shown in Table 1.

perceptible. First, it was noted that the virus concentration in the solution must remain at a sustained high level over a long period of time to achieve sufficient surface coverage. Thus, surface inactivation was found to be negligible in any simulations where the inlet virus concentration was below 10^{13} m^{-3}. Furthermore, only simulations corresponding to a continuous injection of viruses showed any appreciable surface inactivation. Finally, deposition rate coefficients below 10^{-4} m day^{-1} failed to yield sufficient surface coverage to trigger surface inactivation.

To distinguish between the two models of surface inactivation, some continuous injection simulations were performed with a relatively high inlet virus concentration of 1×10^{14} m^{-3}. The simulations were performed for a hydrogeologically uniform aquifer using various rate constants for surface inactivation and keeping the deposition rate constant fixed at 1×10^{-3} m day^{-1}. Virus release was neglected in these simulations after noting that release rate constants smaller than the deposition rate constants did not have any notable influence on the surface coverage. The deposition rate constant used in these simulations are comparable to those for favorable attachment surfaces. Consequently, the virus movement in the domain was considerably restricted resulting in very little virus transport beyond 0.5-m downstream from the inlet.

Fig. 9 shows the evolution of the fractional surface coverage with time corresponding to mechanisms M1 and M2 at an observation location 0.1-m downstream from the inlet. In

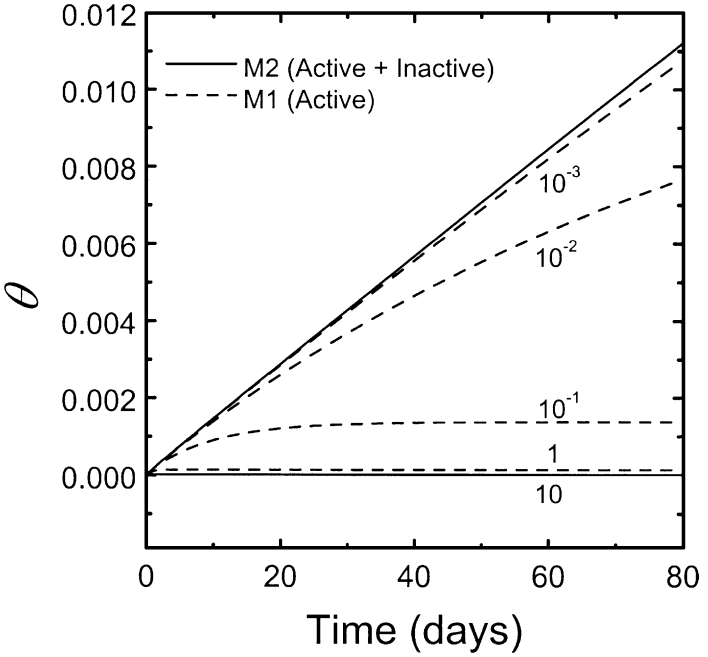

Fig. 9. Time dependence of the fractional surface coverage according to the models M1 and M2 for surface inactivation of viruses. These simulations were performed for continuous line injection of viruses at a high concentration of 10^8 cm^{-3}. The numbers corresponding to the lines represent different surface inactivation rate constants. These profiles were obtained at a location 0.1-m downstream from the left (injection) boundary of the domain. The other various parameters used in the simulations are shown in Table 1.

these simulations, the surface inactivation rate constant was varied over five orders of magnitude as shown in the figure. The solid line represents the total surface coverage due to active and inactive viruses as predicted by the model M2. This total coverage was identical for all of the inactivation rate coefficients used in the simulations. The surface coverage for M1 (which represents the coverage due to the active viruses) varies with the inactivation rate coefficient. For large inactivation rate constants, the coverage is negligible, but as the inactivation rate constant becomes smaller, the surface coverage increases, attaining values similar to M2 in the limit $k_{i,s} < k_a$. For intermediate values of $k_{i,s}$, model M1 predicts a plateau in the surface coverage profile indicating a stationary surface concentration after a few days, while for M2 the surface coverage increases continuously with time. The surface coverages are relatively small in either case, suggesting that the blocking effects are not very important in these regimes of deposition. The increase in surface coverage is more rapid as well as the plateau values of θ are higher for shorter downstream distances from the inlet. This is due to the higher solution phase concentration of viruses near the inlet, which results in greater deposition.

The solution phase virus concentration profiles (or breakthrough curves) corresponding to the two inactivation models are shown in Fig. 10 at two distances from the inlet. These indicate that the mechanism of surface inactivation has very little influence on the solution

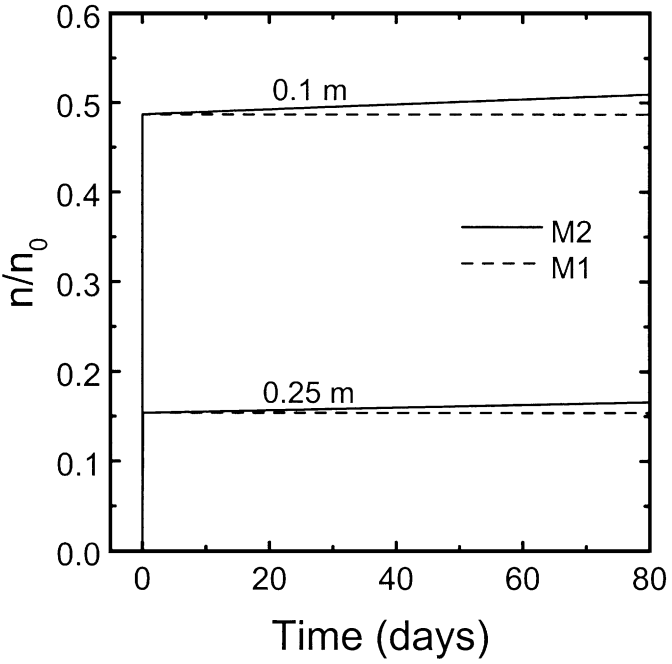

Fig. 10. Comparison of virus breakthrough profiles obtained at two locations 0.1- and 0.25-m downstream from the left boundary of the domain for the two surface inactivation models M1 and M2. The surface inactivation rate coefficients in these simulations were 10 day $^{-1}$. The other various parameters used in the simulations are shown in Table 1.

phase virus concentration profiles. The only notable feature is that for mechanism M1, the concentration profile appears to reach a constant plateau value when the inactivation rate constant is much larger than the deposition rate constant. For mechanism M2, however, we observe a gradual increase in the solution phase concentration over the entire simulation period. The difference between the two mechanisms becomes perceptible only after several days of transport.

The actual process of surface inactivation probably involves a combination of both mechanisms discussed above, although such a detailed modeling may not be necessary to account for a marginal change in the virus concentration distribution in the solution phase. Furthermore, under realistic conditions, virus infiltration may not be continuous over such an extended period of time and the virus concentration at the inlet may be much smaller. In such situations, the secondary mechanisms of surface inactivation will have negligible influence on the overall virus transport.

5. Concluding remarks

The virus transport model presented in this paper is capable of predicting the movement of viruses in a physically and geochemically heterogeneous porous medium. The geo-

chemical heterogeneity in the porous medium is accounted for by a patchwise heterogeneity model. The presence of layered geochemical and physical heterogeneity can significantly affect virus transport in an aquifer. Both layered and randomly distributed physical heterogeneity (hydraulic conductivity) can result in considerable changes in virus movement patterns. Log-normally distributed geochemical heterogeneity with larger variances tends to increase the arithmetic mean value of the heterogeneity parameter, thereby resulting in a slower virus transport. Local variations of the geochemical heterogeneity parameter also cause preferential virus movement, albeit at a smaller length scale.

The model also provides a comprehensive insight into the various modes of virus removal due to attachment (deposition), release, and solution phase and surface inactivation. The virus release and surface inactivation terms depend solely on the surface concentration of the viruses, which in turn, is governed by the rate of virus deposition. Such mechanisms are likely to be insignificant in absence of prolonged virus infiltration in the aquifer at high concentrations. Large virus release rate constants may result in sustained low concentrations in the solution over extended periods of time, resulting in a long-term tail in the breakthrough behavior even after the injection is stopped. The two mechanisms of surface inactivation presented in the study provide different extents of surface coverage, and hence, may influence the virus transport differently, particularly in regions very close to the injection sites. The difference between the two mechanisms, however, is hardly noticeable unless the surface inactivation rate constant is very large. Furthermore, the model simulations show that, under realistic field conditions, surface inactivation has a negligible influence on the overall virus transport compared to inactivation of viruses in solution.

To summarize, the above behaviors suggest that simpler models that account for virus adsorption through a retardation factor may yield a misleading picture of virus transport. In light of the potential hazards posed by only a few virus particles, it is important to accurately track the movement of viruses by comprehensively accounting for every mode of virus removal, release, and inactivation in a transport model. This model, coupled with reliable estimates of the pertinent transport, deposition, inactivation, and release parameters, may lead to adequate prediction of the hydrogeological sensitivity of aquifers.

Acknowledgements

The authors acknowledge the support of US Environmental Protection Agency (EPA Grant R826179, Exploratory Research) and US National Science Foundation (Grants EAR-9418472 and BES-9705717).

References

Abbaszadegan, M., Stewart, P.M., Lechevallier, M.W., Rosen, J.S., Gerba, C.P., 1999. Occurrence of Viruses in Ground Water in the United States. American Water Works Association Research Foundation, Denver, CO.

Bales, R.C., Hinkle, S.R., Kroeger, T.W., Stocking, K., Gerba, C.P., 1991. Bacteriophage adsorption during transport through porous media: chemical perturbations and reversibility. Environ. Sci. Technol. 25, 2088–2095.

Bear, J., 1988. Dynamics of Fluids in Porous Media. Dover Publications, New York.

Bitton, G., Harvey, R.W., 1992. Transport of pathogens through soils and aquifers. In: Mitchell, R. (Ed.), Environmental Microbiology. Wiley-Liss, New York, pp. 103–124.

Chrysikopoulos, C.V., Sim, Y., 1996. One-dimensional virus transport in homogeneous porous media with time-dependent distribution coefficient. J. Hydrol. 185, 199–219.

Dagan, G., 1989. Flow and Transport in Porous Formations. Springer-Verlag, New York.

Derjaguin, B.V., Landau, L., 1941. Theory of the stability of strongly charged lyophobic sols and the adhesion of strongly charged particles in solutions of electrolytes. Acta Physicochim. URSS 14, 633–662.

Dowd, S.E., Pillai, S.D., Wang, S.Y., Corapcioglu, M.Y., 1998. Delineating the specific influence of virus isoelectric point and size on virus adsorption and transport through sandy soils. Appl. Environ. Microbiol. 64 (2), 405–410.

Elimelech, M., Gregory, J., Jia, X., Williams, R.A., 1995. Particle Deposition and Aggregation: Measurement, Modelling and Simulation. Butterworth-Heinemann, Oxford.

Elimelech, M., Nagai, M., Ko, C.-H., Ryan, J.N., 2000. Relative insignificance of mineral grain zeta potential to colloid transport in geochemically heterogeneous porous media. Environ. Sci. Technol. 34, 2143–2148.

Gelhar, L.W., Axness, C.L., 1983. Three-dimensional stochastic analysis of macrodispersion in aquifers. Water Resour. Res. 19 (1), 161–180.

Gerba, C.P., 1984. Applied and theoretical aspects of virus adsorption to surfaces. Adv. Appl. Microbiol. 30, 133–169.

Grant, S.B., List, E.J., Lidstrom, M.E., 1993. Kinetic analysis of virus adsorption and inactivation in batch experiments. Water Resour. Res. 29 (7), 2067–2085.

Happel, J., 1958. Viscous flow in multiparticle systems—slow motion of fluids relative to beds of spherical particles. AIChE J. 4 (2), 197–201.

Ibaraki, M., Sudicky, E.A., 1995a. Colloid-facilitated contaminant transport in discretely fractured porous media: 1. Numerical formulation and sensitivity analysis. Water Resour. Res. 31 (12), 2945–2960.

Ibaraki, M., Sudicky, E.A., 1995b. Colloid-facilitated contaminant transport in discretely fractured porous media: 2. Fracture network examples. Water Resour. Res. 31 (12), 2961–2969.

Johnson, P.R., Elimelech, M., 1995. Dynamics of colloid deposition in porous media: blocking based on random sequential adsorption. Environ. Sci. Technol. 11, 801–812.

Johnson, P.R., Sun, N., Elimelech, M., 1996. Colloid transport in geochemically heterogeneous porous media: modeling and measurements. Environ. Sci. Technol. 30, 3284–3293.

Knapp, E.P., Herman, J.S., Hornberger, G.M., Mills, A.L., 1998. The effect of distribution of iron-oxyhydroxide grain coatings on the transport of bacterial cells in porous media. Environ. Geol. 33, 243–248.

Ko, C.-H., Bhattacharjee, S., Elimelech, M., 2000. Coupled influence of colloidal and hydrodynamic interactions on the RSA dynamic blocking function for particle deposition onto packed spherical collectors. J. Colloid Interface Sci. 229, 554–567.

Kuhnen, F., Barmettler, K., Bhattacharjee, S., Elimelech, M., Kretzschmar, R., 2000. Transport of iron oxide colloids in packed quartz sand media: monolayer and multilayer deposition. J. Colloid Interface Sci. 231, 31–41.

Liew, P.-F., Gerba, C.P., 1980. Thermostabilization of enteroviruses by estuarine sediments. Appl. Environ. Microbiol. 40, 305–308.

Loveland, J.P., Ryan, J.N., Amy, G.L., Harvey, R.W., 1996. The reversibility of virus attachment to mineral surfaces. Colloids Surf., A: Physicochem. Eng. Aspects 107, 205–221.

Mantoglou, A., Wilson, J.L., 1982. The turning bands method for simulation of random fields using line generation by a spectral method. Water Resour. Res. 18 (5), 1379–1394.

Murray, J.P., Labland, S.J., 1979. Degradation of poliovirus by adsorption on inorganic surfaces. Appl. Environ. Microbiol. 37 (3), 480–486.

Murray, J.P., Parks, G.A., 1980. Poliovirus adsorption on oxide surfaces. Correspondence with the DLVO-Lifshitz theory of colloid stability. In: Kavanaugh, M.C., Leckie, J.O. (Eds.), Particulates in Water. Characterization, Fate, Effects, and Removal. American Chemical Society, Washington, DC, pp. 97–133.

Navigato, T.N., 1999. Effect of attachment to ferric oxyhydroxide-coated sand on the inactivation of bacteriphages PRD1 and MS2. MS Thesis, University of Colorado, Boulder, 147 pp.

Park, N.-S., Blandford, T.N., Huyakorn, P.S., 1992. VIRALT, Version 2.1, Documentation and User's Guide HydroGeoLogic, Herndon, VA.

Park, N.-S., Blandford, T.N., Wu, Y.-S., Huyakorn, P.S., 1993. CANVAS: a composite analytical-numerical model for viral and solute transport simulation. Documentation and User's Guide, Version 1.0. HydroGeo-Logic, Herndon, VA.

Penrod, S.L., Olson, T.M., Grant, S.B., 1996. Deposition kinetics of two viruses in packed beds of quartz granular media. Langmuir 12, 5576–5587.

Pieper, A.P., 1995. Groundwater Transport of Viruses: A Natural Gradient Field Test in a Contaminated Sandy Aquifer. MS Thesis, University of Colorado, Boulder.

Rajagopalan, R., Tien, C., 1976. Trajectory analysis of deep-bed filtration with the sphere-in-cell porous media model. AIChE J. 22, 523–533.

Rehmann, L.L.C., Welty, C., Harvey, R.W., 1999. Stochastic analysis of virus transport in aquifers. Water Resour. Res. 35 (7), 1987–2006.

Ren, J., Packman, A.I., Welty, C., 2000. Correlation of colloid collision efficiency with hydraulic conductivity of silica sands. Water Resour. Res. 36, 2493–2500.

Rubin, Y., 1990. Stochastic modeling of macrodispersion in heterogeneous porous media. Water Resour. Res. 26 (1), 133–141.

Ryan, J.N., Elimelech, M., Ard, R.A., Harvey, R.W., Johnson, P.R., 1999. Bacteriophage PRD1 and silica colloid transport and recovery in an iron oxide-coated sand aquifer. Environ. Sci. Technol. 33, 63–73.

Schijven, J.F., Hassanizadeh, S.M., 2000. Removal of viruses by soil passage: overview of modeling, processes, and parameters. Crit. Rev. Environ. Sci. Technol. 30 (1), 49–127.

Schijven, J.F., Hoogenboezem, W., Hassanizadeh, S.M., Peters, J.H., 1999. Modeling removal of bateriophages MS2 and PRD1 by dune recharge at Castricum, Netherlands. Water Resour. Res. 35, 1101–1111.

Schijven, J.F., Medema, G.J., Vogelaar, A.J., Hassanizadeh, S.M., 2000. Removal of microorganisms by deep well injection. J. Contam. Hydrol. 44, 301–327.

Scholl, M.A., Harvey, R.W., 1992. Laboratory investigation on the role of sediment surface and groundwater chemistry in transport of bacteria through a contaminated sandy aquifer. Environ. Sci. Technol. 26, 1410–1417.

Song, L., Elimelech, M., 1993. Dynamics of colloid deposition in porous media: modeling the role of retained particles. Colloids Surf., A: Physicochem. Eng. Aspects 73, 49–63.

Song, L., Elimelech, M., 1994. Transient deposition of colloidal particles in heterogeneous porous media. J. Colloid Interface Sci. 167, 301–313.

Song, L., Johnson, P.R., Elimelech, M., 1994. Kinetics of colloid deposition onto heterogeneously charged surfaces in porous media. Environ. Sci. Technol. 28, 1164–1171.

Stagg, C.H., Wallis, C., Ward, C.H., 1977. Inactivation of clay-associated bacteriophage MS-2 by chlorine. Appl. Environ. Microbiol. 33, 385–391.

Sun, N.Z., 1995. Mathematical Modeling of Groundwater Pollution. Springer-Verlag, Berlin.

Sun, N.-Z., Yeh, W.W.G., 1983. A proposed upstream weight numerical method for simulating pollutant transport in groundwater. Water Resour. Res. 19, 1489–1500.

Sun, N., Elimelech, M., Sun, N.-Z., Ryan, J.N., 2001. A novel two-dimensional model for colloid transport in physically and geochemically heterogeneous porous media. J. Contam. Hydrol. 49, 173–199.

Taylor, D.H., Moore, R.S., Sturman, L.S., 1981. Influence of pH and electrolyte composition on adsorption of poliovirus by soils and minerals. Appl. Environ. Microbiol. 42, 976–984.

Tim, U.S., Mostaghimi, S., 1991. Model for predicting virus movement through soils. Ground Water 29, 251–259.

Tompson, A.F.B., Ababou, R., Gelhar, L.W., 1989. Implementation of the three dimensional turning bands random field generator. Water Resour. Res. 25 (10), 2227–2243.

US Environmental Protection Agency, 2000. National Primary Drinking Water Regulations: Ground Water Rule; Proposed Rules. 40 CFR Parts 141 and 142.

Verwey, E.J.W., Overbeek, J.T.G., 1948. Theory of the Stability of Lyophobic Colloids. Elsevier, Amsterdam.

Vilker, V.L., Burge, W.D., 1980. Adsorption mass transfer model for virus transport in soils. Water Res. 14, 783–790.

Yao, K.-M., Habibian, M.T., O'Melia, C.R., 1971. Water and wastewater treatment filtration: concepts and applications. Environ. Sci. Technol. 5, 1105–1112.

Yates, M.V., 1995. Field evaluation of the GWDR's natural disinfection criteria. J. Am. Water Works Assoc. 87, 76–85.

Yates, M.V., Gerba, C.P., Kelley, L.M., 1985. Virus persistence in groundwater. Appl. Environ. Microbiol. 49, 778–781.

Yates, M.V., Yates, S.R., Wagner, J., Gerba, C.P., 1987. Modeling virus survival and transport in the subsurface. J. Contam. Hydrol. 1, 329–345.

Zerda, K.S., Gerba, C.P., Hou, K.C., Goyal, S.M., 1985. Adsorption of viruses to charge-modified silica. Appl. Environ. Microbiol. 49, 91–95.